Anchoring Sites for Initial Au Nucleation on CeO_2{111}: O Vacancy versus Ce Vacancy

Changjun Zhang,[†] Angelos Michaelides,[‡] David A. King,[†] and Stephen J. Jenkins*[,†]

Department of Chemistry, University of Cambridge, Lensfield Road, Cambridge, CB2 1EW, U.K., and Materials Simulation Laboratory, London Centre for Nanotechnology & Department of Chemistry, University College London, London, WC1H 0AH, U.K.

Received: November 17, 2008; Revised Manuscript Received: February 5, 2009

Gold atoms act as anchoring sites for gold nanoparticles in the ceria-catalyzed water−gas shift reaction; however, the anchoring site of the nanoparticle is a matter of debate. Both oxygen and cerium vacancies have been suggested as the anchoring sites in different studies. Aiming to provide insight into this issue, we utilize density functional theory and ab initio thermodynamics approaches to investigate the formation of various vacancies at a CeO_2{111} surface, both with and without gold adatoms. We find that, under reaction conditions, the cerium vacancy is much harder to form and is much less stable than the oxygen vacancy, regardless of the absence or presence of gold on the surface. Gold adsorption at the oxygen vacancy site is strongly preferred to that on the cerium vacancy; the latter becomes favorable only near the extreme oxygen-rich limit, which would not be achievable under the reaction conditions. Other possible vacancies have also been examined. We find that in addition to a single oxygen vacancy, oxygen vacancy clusters could also be anchoring sites for gold nucleation. This study lays a foundation toward understanding the boundary structure between Au nanoparticlues and ceria support, which in turn would hold promise to unravel their catalytic roles.

I. Introduction

Ceria-supported gold catalysts have recently attracted much research interest, primarily due to their excellent catalytic activity reported for the water−gas shift (WGS) reaction, which is a crucial step in many applications such as the production of hydrogen for fuel cells.[1−6] Despite extensive studies, some questions concerning the nature of the gold nanoparticle on ceria remain open. In addition to the vigorous debate of the nature of the active form of gold (i.e., metallic versus ionic) in the literature, controversies also exist for the issue of the location of the gold nanoparticle.[7] The formation of the nanoparticle is often thought to be seeded at gold atoms embedded into the ceria lattice, so that the nanoparticle can be resistant to sintering and does not lose its integrity. However, different anchoring sites for the nanoparticle have been proposed, either locked into an O vacancy or into a Ce vacancy. Recognizing that gold would exhibit distinct electronic features on these vacancies, a definitive answer of its location is important in interpreting the nature of the active site(s) and consequently different WGS mechanisms.

Given the well-known high oxygen transport and storage capacities of ceria, O vacancies in ceria are naturally anticipated in catalytic processes. Indeed, many studies have suggested the existence and the importance of O vacancies in Au/CeO_2 catalysts. For example, Tabakova et al.[8] observed an absorbance band at 2060 cm^{-1} in their infrared spectroscopy study, which was assigned to CO adsorbed on a $Au^{\delta-}$ site. The presence of $Au^{\delta-}$ was attributed to the effect of O vacancies, because these would allow electron transfer to the Au to occur. By using synchrotron-based photoemission, Rodriguez et al.[9,10] observed a Ce^{3+} peak in the spectra for Au/CeO_2{111}, also indicative of the presence of O vacancies, and they further suggested that the active sites should involve small Au clusters in close contact with O vacancies. Although those experiments provide little information of the boundary structure between Au clusters and ceria, the conventional view assumes the oxygen vacancy model,[11] namely, the anchoring of metal clusters in the O vacancies created at the surface of the support. Density functional theory (DFT) calculations have added significantly to the understanding of the boundary structure between Au clusters and O vacancies. Liu et al.[12] found strong interaction between an individual Au atom and an O vacancy on CeO_2{111} and showed further that this Au atom, occupying the O vacancy itself, can act as the nucleation site for the growth of a small cluster, which facilitates the WGS reaction.

In contrast, Tibiletti et al.[13] proposed, in a combined experimental and theoretical study, that the Au nanoparticle is anchored via a cationic Au atom at a cerium vacancy on CeO_2{111} (i.e., the Ce vacancy model). The two main pieces of evidence put forward in that study were (i) that the calculated structure of Au at the O vacancy site does not agree with their extended X-ray absorption fine structure (EXAFS) experiment and (ii) that Au at the Ce vacancy site has more negative (i.e., stronger) adsorption energy (−5.6 eV) than that at the O vacancy site (−2.5 eV). Considering the first point, we note that only a single Au atom was considered in their calculations, which might be inadequate to compare with the EXAFS data (i.e., the reported Au−O and Au−Ce distances). In fact, calculated results of those distances from a single Au atom adsorbed on the perfect stoichiometric {111} surface could *also* have a seemingly good agreement with experiments, so this evidence is not conclusive in itself. Considering the second point concerning the adsorption energies, their results were calculated with respect to the relevant defective surfaces, either with a pre-existing Ce vacancy or a pre-existing O vacancy. Questions must therefore arise here about under what conditions the Ce vacancy would form and about how the adsorption energy varies when taking the vacancy formation into account. Without including the effect from the vacancy formation, the energy results are likely to be misleading.

* Author to whom correspondence should be addressed. E-mail: sjj24@cam.ac.uk.
[†] University of Cambridge.
[‡] University College London.

10.1021/jp810093a CCC: $40.75
Published on Web 03/30/2009

Another piece of evidence in the literature to support the Ce vacancy model comes from an X-ray diffraction study:[14] a slightly contracted lattice constant was observed for Au-doped ceria, which was then interpreted as partial lattice filling of vacant Ce sites with Au. However, we find that the lattice would also be slightly contracted in the case of O vacancies, and thus, this evidence is not conclusive either. In addition, it is also worth mentioning that, in recent theoretical studies of Au-doped ceria surfaces,[15−17] Au was assumed to be on the Ce vacancy site, based on those pieces of "evidence". Clearly, the validity of the Ce vacancy model needs to be clarified.

In the current work, we have therefore undertaken a theoretical investigation of vacancy formation and Au adsorption. We aim to establish under what conditions different vacancies would occur and how that would be altered by the addition of Au. Not only do we calculate energetics directly from DFT, more importantly, we also consider the free energy. The latter is essential in examining the stability of a surface in equilibrium with a given environment at finite temperature and pressure and thus would be able to provide a more realistic description of the system. To this end, we adopt the approach of combining DFT energetics and thermodynamics, known as ab initio thermodynamics, which has lately been a valuable tool in addressing many stability issues in solid state areas.[18−21] In addition to O and Ce vacancies, we also consider some other vacancies, including a vacancy containing a unit of CeO_2 and also O vacancy clusters, which could have interesting implications for the issue of anchoring sites.

II. Computational Details

We carry out spin-polarized calculations within the DFT framework, as implemented in the Vienna Ab Initio Simulation Program (VASP), a widely used plane-wave pseudopotential DFT package.[22−24] We use the projector-augmented wave method to describe the effect of the core electrons on the valence electrons in the system.[25,26] The Ce 5s, 5p, 5d, 4f, and 6s electrons; the O 2s and 2p electrons; and the Au 5d, 6s, and 6p electrons are treated as valence electrons. For the electron exchange-correlation functional, the generalized gradient approximation (GGA) of Perdew and Wang[27] is used.

We choose the DFT+U methodology,[28,29] which has proven useful in descriptions of ceria systems. In this approach, the Hubbard parameter, U, is introduced to account for the strong on-site Coulomb repulsion among the localized Ce 4f electrons. In practice, however, the choice of this parameter is often empirical, which is to say that the U value is adjusted to reproduce properties known in experiments. There are a host of papers devoted to the discussion of appropriate U values.[30−35] In studying reduced ceria, Nolan et al.[30] suggested $U = 5.0$ eV for GGA+U, as for $U < 5.0$ eV significant delocalization still persists; Fabris et al.[31] derived $U = 5.3$ eV for LDA and $U = 4.5$ eV for GGA+U when using the more advanced maximally localized Wannier orbitals as the projector functions; Andersson et al.[34] showed that $U \approx 6.0$ eV for LDA+U and $U \approx 5.0$ eV for GGA+U provide a consistent description of pure CeO_2 and Ce_2O_3 plus vacancies in CeO_2; Castleton et al.[35] also suggested that the best overall choice is $U \approx 6.0$ eV for LDA+U and $U \approx 5.5$ eV for GGA+U. We note that although suggestions of U values vary, the optimal ones appear to be around 5.0 eV for GGA+U and 6.0 eV for LDA+U. We have performed GGA+U calculations with a range of U values ($U = 2.0$, 3.0, 4.0, 5.0, 5.5, 6.0, and 7.0 eV) in this work. We find that on the reduced surface with an O vacancy, the two excess electrons left behind by the removed O starts to become localized at $U = 3.0$ eV; the degree of localization reaches a maximum at $U = 5.0$ eV; for higher U values the charge localized at Ce ions decreases, all of which are consistent with previous studies.[30,35] We have also examined the dependence of important properties, such as vacancy formation energies and Au adsorption energies, on the U values and DFT functionals, which will be presented below. Our results show that despite some variations in the energies, the relative stabilities of different vacancies are not overly dependent on those choices in the calculations. Therefore, the discussion on the thermodynamics will be made with the results from GGA+U ($U = 5.0$ eV) calculations.

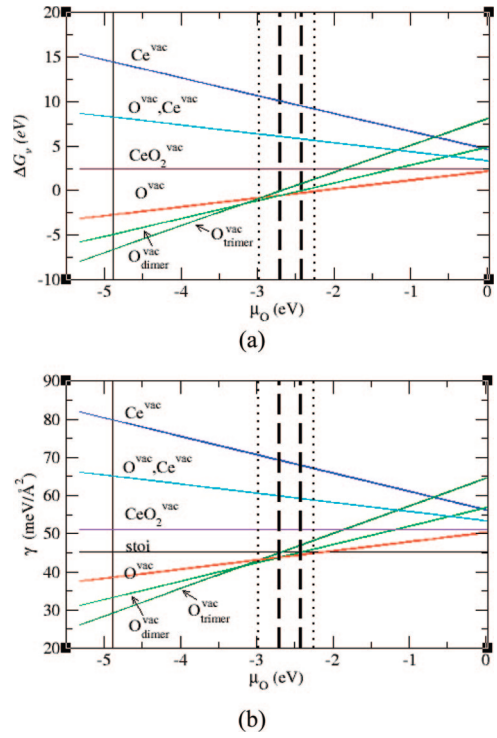

Figure 1. Vacancy formation energy (ΔG_v) and surface energy (γ) as a function of O chemical potential (μ_O). Ce^{vac}; O^{vac},Ce^{vac}; CeO_2^{vac}; stoi; O^{vac}; O^{vac}_{dimer}; and O^{vac}_{trimer} represent results from surfaces with a Ce vacancy, an O and a Ce vacancy, a CeO_2 vacancy, no vacancy, an O vacancy, an O vacancy dimer, and an O vacancy trimer, respectively. The vertical solid line refers to the O-poor limit, and the zero point of the x-axis refers to the O-rich limit. The region between the two vertical dashed lines represents those values of μ_O under typical water−gas shift reaction conditions (see the text). The region between the two vertical dotted lines represents those values of μ_O calculated with a broad range of partial pressures (see also the text).

The {111} face of ceria, chosen in this study, features an oxygen termination of stoichiometric O−Ce−O trilayers stacked along the [111] direction and is the thermodynamically most stable surface. A large (4 × 4) unit cell of the CeO_2{111} surface is used in our calculations so that the vacancy interaction between cells is small. Our surface models contain nine atomic layers (or three trilayers of CeO_2 units), i.e., including up to 144 atoms, and ~12 Å vacuum regions. Tests performed on a 12-layer slab show that vacancy formation energies vary within the region of 0.05 eV. All atoms were allowed to relax until the forces were smaller than 0.02 eV/Å, except those in the lower-most three layers that were constrained to the equilibrium positions calculated for the defect-free supercell. We have also performed variable cell calculations and found very small cell relaxations (lattice contractions are similar for surfaces containing an O vacancy or a Ce vacancy, being ~0.2%) and very small effect on the energy differences (~0.1 eV). The sampling

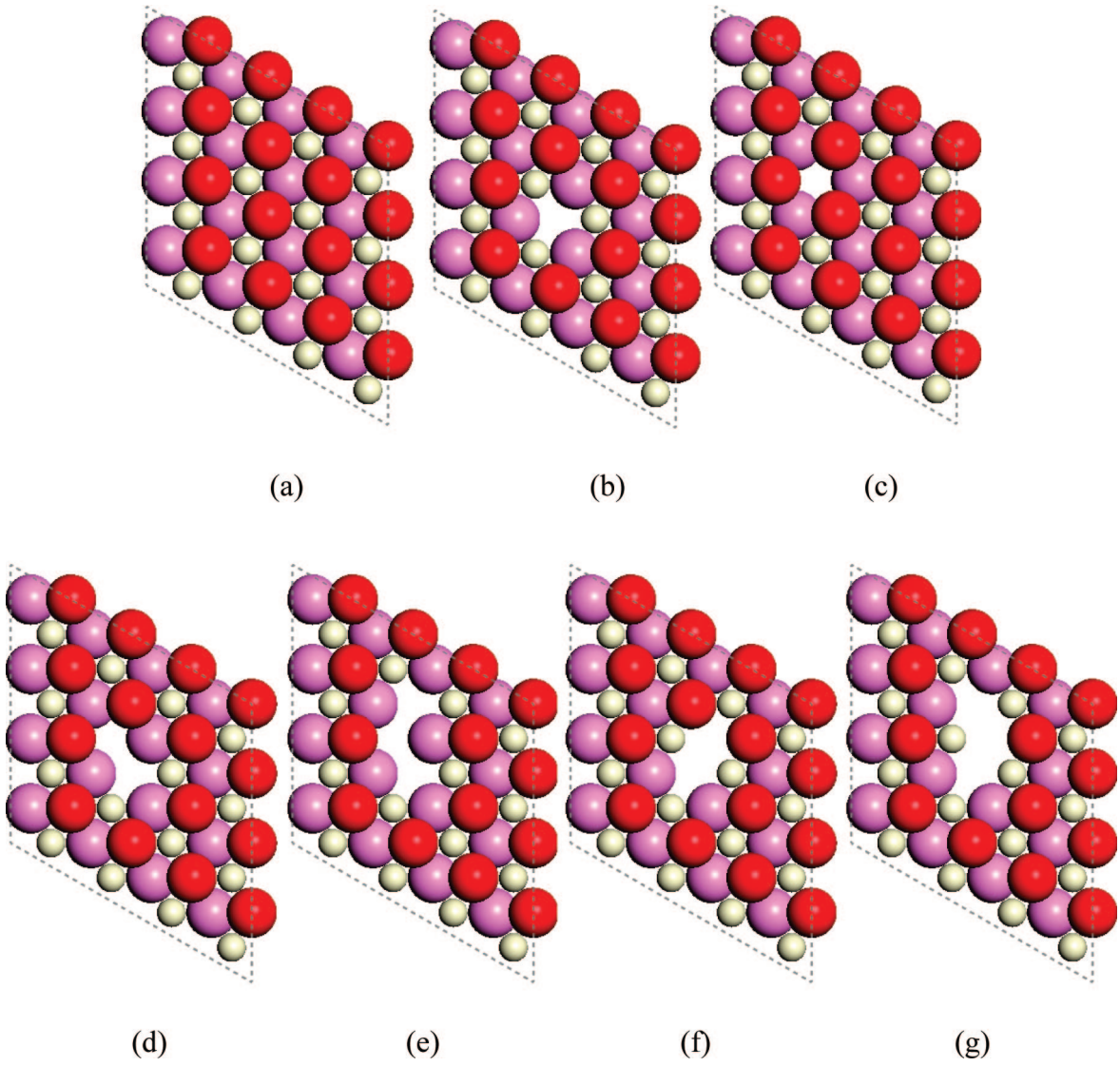

Figure 2. Structures of surfaces (a) with no vacancy (i.e., the stoichiomtric surface), (b) with an O vacancy, (c) with a Ce vacanc,; (d) with an O and a Ce vacancy, (e) with a CeO_2 vacancy, (f) with an O vacancy dimer, and (g) with an O vacancy trimer. Surface O atoms are in red, subsurface O atoms are in pink, and Ce atoms are in gray. For clarity, only the top three layers of the surfaces are shown.

of the Brillouin zone was performed with a 2 × 2 × 1 Monkhorst-Pack *k*-point mesh, and the number of plane waves, used to expand the Kohn−Sham orbitals, is controlled by a cutoff energy of 400 eV, which are sufficient to obtain well-converged energies.[36]

III. Results and Discussion

We consider the surfaces in contact with an oxygen atmosphere, which acts as a thermodynamic reservoir and can be described by the oxygen chemical potential (μ_O), through which the temperature and pressure effects on the free energy of O_2 are included. We note that μ_O can be expressed as

$$\mu_O(T,p) = \frac{1}{2}\left[\mu_{O_2}(T,p^0) + k_B T \ln\left(\frac{p_{O_2}}{p^0}\right)\right] \quad (1)$$

where $\mu_{O_2}(T,p^0)$ includes the contributions from rotations and vibrations of the molecule as well as the ideal-gas entropy at $p^0 = 1$ atm. If the zero reference state of $\mu_{O_2}(T,p^0)$ is chosen to be the total DFT energy of an O_2 molecule [i.e., $\mu_{O_2}(0K,p^0) = E_{O_2}^{total} \equiv 0$], we can calculate $\mu_{O_2}(T,p^0)$ from

$$\mu_{O_2}(T,p^0) = \Delta H_{O_2}(T \rightarrow T^0, p^0) - T\Delta S_{O_2}(T \rightarrow 0K, p^0) + \Delta H_{O_2}(T^0 \rightarrow 0K, p^0) \quad (2)$$

where ΔH_{O_2} and ΔS_{O_2} are the experimental values listed in the thermodynamic tables.[37] We note that $\mu_O(T,p)$ is subject to the following boundary conditions, $^1/_2\Delta G_f^{CeO_2}(0,0) < \mu_O < {}^1/_2E_{O_2}^{total}$, where $\Delta G_f^{CeO_2}(0,0)$ is the formation energy of the CeO_2 crystal at zero temperature and pressure.[16] The values of $^1/_2\Delta G_f^{CeO_2}$and $^1/_2E_{O_2}^{total}$ refer respectively to the oxygen-poor limit and the oxygen-rich limit conditions. We compute $\Delta G_f^{CeO_2}(0,0)$ to be 9.76 eV, which is consistent with previously reported results.[38] Thus, with respect to $E_{O_2}^{total}$, μ_O must lie in the range from −4.88 to 0.0 eV. We also note that μ_O is not independent but associated with the chemical potentials of other substances involved in the WGS reaction. When the reaction is at equilibrium, μ_O can be given by $\mu_{H_2O} - \mu_{H_2}$, where μ_{H_2O} and μ_{H_2} are chemical

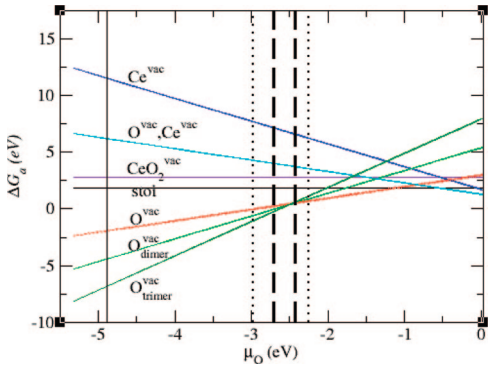

Figure 3. Free energy of Au adsorption (ΔG_a) as a function of O chemical potential (μ_O). Ce^{vac}; O^{vac},Ce^{vac}; CeO_2^{vac}; stoi; O^{vac}; O^{vac}_{dimer}; and O^{vac}_{trimer} represent results from surfaces with a Ce vacancy, an O vacancy and a Ce vacancy, a CeO_2 vacancy, no vacancy, an O vacancy, an O vacancy dimer, and an O vacancy trimer, respectively. The vertical solid line refers to the O-poor limit and the zero point of the *x*-axis refers to the O-rich limit. The region between the two vertical dashed lines represents those values of μ_O under typical water−gas shift reaction conditions (see the text). The region between the two vertical dotted lines represents those values of μ_O calculated with a broad range of partial pressures (see also the text).

potentials of water and hydrogen, respectively, which each can be expressed in a similar manner to that used for μ_O. Thus, from WGS reaction conditions (namely, temperature at ∼400−800 K and partial pressures of H_2O and H_2 at ∼20 and ∼40 kPa, respectively[39,40]), we compute μ_O to lie in the range from −2.71 to −2.43 eV, which is near the midway between the extreme O-poor and the O-rich limits. We also measure the effect on the μ_O values from varying partial pressures of H_2O and H_2 in a large region (from 1 to 100 kPa), which is a random choice, but might be viewed as the error bar for the partial pressures. We find that μ_O would lie in between −2.98 and −2.25 eV, which is quite close to the original range calculated with the experimentally reported partial pressures. In our later discussion, we will see that, even in this broader region, our conclusions are still valid.

A. Vacancy Formation. Having determined the values of μ_O, we can now examine the important thermodynamic properties of vacancy formation energy [$\Delta G_v(T,p)$] and surface energy [$\gamma(T,p)$], which would reveal the feasibility of creating vacancies and the stability of the formed vacancies. Under the assumption that there is enough bulk oxide to act as thermodynamic reservoir,[18] we write

$$\Delta G_v(T,p) = E_{slab} - E_{stoi} + N_O^{vac}\mu_O(T,p) + N_{Ce}^{vac}[e_{CeO_2}^{bulk} - 2\mu_O(T,p)] \quad (3)$$

for the vacancy formation energy and

$$\gamma(T,p) = [(E_{slab} - N_{Ce}e_{CeO_2}^{bulk} + (2N_{Ce} - N_O)\mu_O(T,P)]/A \quad (4)$$

for the surface free energy, where E_{stoi}, E_{slab}, and $e_{CeO_2}^{bulk}$ are the DFT energies of the stoichiometric surface, of the defective surface under consideration, and of a formula unit of the bulk, respectively, N_O^{vac} and N_{Ce}^{vac} are the numbers of Ce and O vacancies, respectively, N_O and N_{Ce} are the numbers of Ce and O atoms in the system, respectively, and A is the area of the surface cell. We note that the finite temperature and pressure effects on the stoichiometric and defective surfaces are ignored in the above equations; such approximations are commonly used and justified.[18,19] Taking the vibrational contribution to the free energies (F) as an example, it can be written as an integral over the modes ω

$$F = \int F^{vib}(T,\omega)\,\sigma(\omega)\,d\omega \quad (5)$$

where $\sigma(\omega)$ is the phonon density of state (DOS) and the function $F^{vib}(T,\omega)$ is described explicitly in ref 18. To estimate F, the phonon DOS is represented by one characteristic frequency for each atom type (ϖ_{Ce} and ϖ_O, possibly varying slightly at the surface), and thus eq 5 is simplified to an analytical expression in ϖ_{Ce} and ϖ_O. From this approximation, the vibrational contribution to the free energies of a RuO_2 system was previously calculated to be small and thus neglected.[18] In the case of CeO_2, we expect that ϖ_{Ce} and ϖ_O could be close to ϖ_{Ru} and ϖ_O, respectively (the latter two modes are known in the literature), since the square root of the mass ratio (Ce:Ru) is close to 1. The results for RuO_2 are therefore quite applicable to our case. In the temperature range of interest in this study (400−800 K), this means that the vibrational contribution to the surface free energy is less than 7.0 meV/Å^2,[18] which, as will be seen shortly, would not affect our conclusions. We should mention that although this seems to be a rough estimate for the vibrational modes, a variation (as large as 50%) of all the vibration modes would still predict the largest vibrational contribution to be ∼7.0 meV/Å^2 in the temperature range, as demonstrated clearly in ref 18.

Figure 1 shows striking differences of ΔG_v (and γ) between surfaces with an O vacancy and a Ce vacancy. Under reaction conditions (i.e., $-2.7 < \mu_O < -2.4$ eV depicted by dotted rectangular areas), it requires an enormous amount more energy (∼10 eV) to create a Ce vacancy than to create an O one. The surface with a Ce vacancy is ∼30 meV/Å^2 less stable than that with an O vacancy: the difference is also very large given that γ for the stoichiometric surface is 45 meV/Å^2 (this surface energy value is very close to that reported for the stoichiometric surface in ref 31). Of course, an increase in μ_O (i.e., an increase in the partial pressure of O or a decrease in temperature) would favor the Ce vacancy formation. However, even at the O-rich limit, it is still much harder to create a Ce vacancy than an O vacancy, and the surface with the Ce vacancy is still much less stable.

We also consider a defect containing both an O and a Ce vacancy and a defect containing two O and one Ce vacancy (i.e., a formula unit of CeO_2). Both defects (Figure 2d,e) are found to be more stable than a single Ce vacancy (Figure 2b). This is because the creation of a single Ce vacancy leads to significant charge depletions on the seven O atoms surrounding the Ce vacancy,[36] whereas a further removal of an O atom would leave two excess electrons that could compensate the charge loss to some extent; in particular, the surface with a CeO_2 vacancy is able to maintain the electron neutrality and thus is the most stable among the three defects. Because the ratio of N_O:N_{Ce} remains stoichiometric for the surface with a CeO_2 vacancy, ΔG_v and γ in this case are independent of μ_O. Nevertheless, we note from Figure 1 that under reaction conditions, ΔG_v in forming a CeO_2 vacancy is still ∼3 eV larger than that in forming an O vacancy. Only near the O-rich limits does the formation of a CeO_2 vacancy become competitive against the formation of an O vacancy.

We also plot, in Figure 1, ΔG_v and γ for the surfaces containing an O vacancy dimer or an O vacancy trimer, which

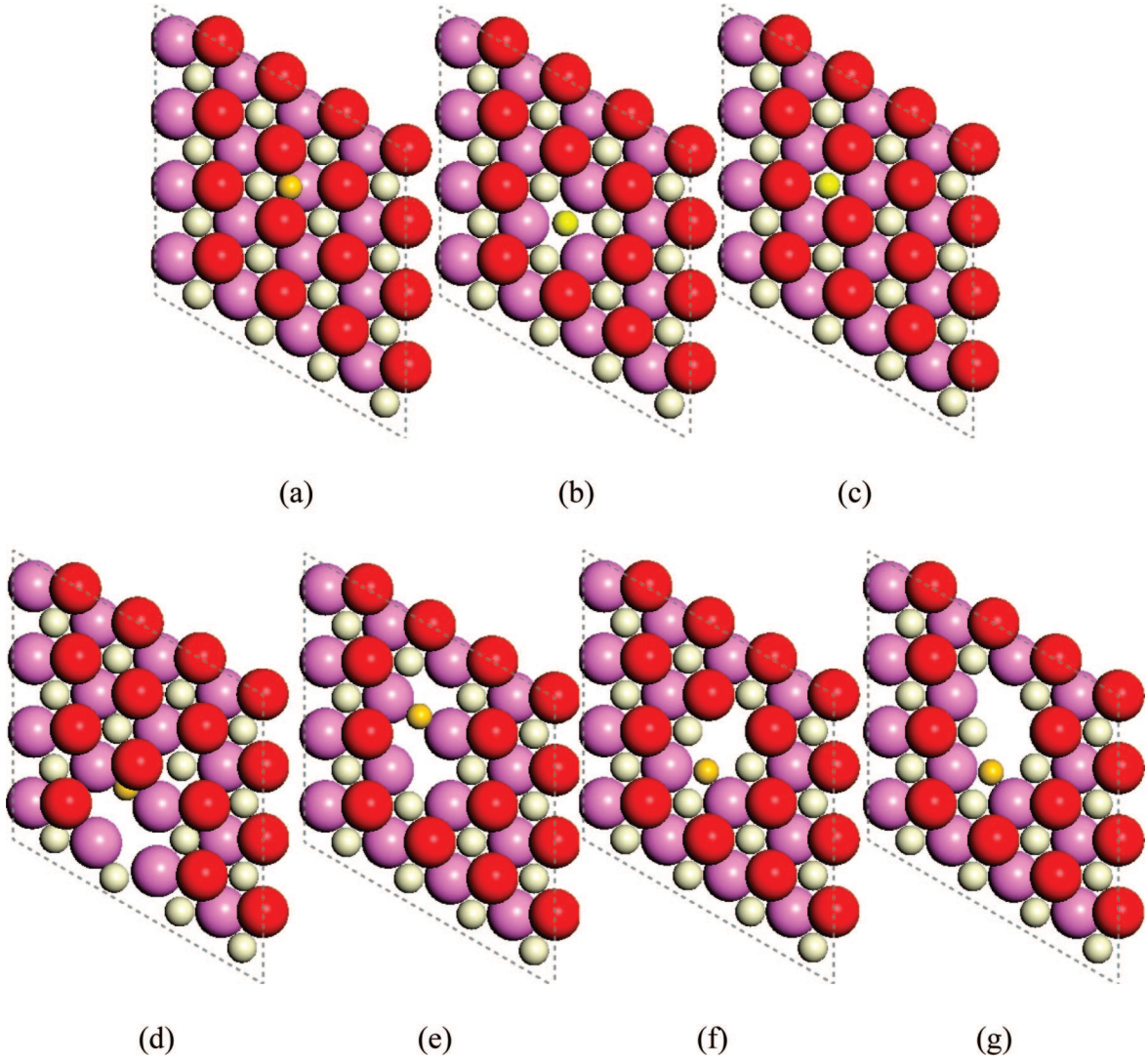

Figure 4. Structures of Au adsorption on various surfaces: (a) with no vacancy (i.e., the stoichiomtric one), (b) with an O vacancy, (c) with a Ce vacancy, (d) with an O and a Ce vacancy, (e) with a CeO_2 vacancy, (f) with an O vacancy dimer, and (g) with an O vacancy trimer. The Au atom is in yellow, and the color coding for the other atoms is the same as in Figure 2.

were observed along with the single O vacancy in scanning tunneling microscopy images.[41] In our calculations, the experimentally reported structures are used, in which a subsurface O vacancy is involved (Figure 2f,g). Compared to that for the single surface O vacancy, the energy dependences on μ_O become more prominent in the cases of vacancy clusters (i.e., the slopes of ΔG_v and γ are larger). Interestingly, under WGS conditions, values of ΔG_v and γ for the surfaces with the O vacancy clusters are close to those for the surface with a single O vacancy, suggesting that the O vacancy clusters could be present along with the single O vacancy.

B. Addition of Au. We turn now to examine Au on various surface sites by computing free energies of Au atom adsorption (ΔG_a), which are given by

$$\Delta G_a(T,p) = E_{slab}^{Au} - E_{stoi} + N_O^{vac}\mu_O(T,p) + N_{Ce}^{vac}[e_{CeO_2}^{bulk} - 2\mu_O(T,P)] - \mu_{Au}(T,p) \quad (6)$$

where μ_{Au} represents the chemical potential of Au, set as the total energy of a Au atom in the bulk fcc crystal, and the rest of the terms are self-explanatory. This free energy is measured relative to the stoichiometric surface and so includes the energy cost of creating whatever vacancy the Au atom may be associated with. It is worth mentioning that the free energy of adsorption can also be viewed as the surface vacancy formation energy in the presence of Au. Thus, by comparing ΔG_a and ΔG_v, we can assess how the addition of Au alters the thermodynamic stability of the defects. From Figure 1 to Figure 3, the energy differences between surfaces with an O vacancy and with a Ce vacancy are lowered by ~3 eV, which is obviously due to the stronger bonding of Au at the Ce vacancy site than that at the O vacancy site (as calculated from DFT).

From Figure 3, we see clearly that, under WGS conditions, adsorption at O vacancy sites are the most stable and that Au at a single O vacancy (Figure 4b) and Au at vacancy clusters (still occupying an O vacancy site in Figure 4f and 4g) have almost equal stabilities because of the similar ΔG_a values. The next most stable adsorption (Figure 4a) is on the stoichiometric surface, via a surface bridgelike site (the most favorable site),[36] which is ~1.7 eV higher in energy than on the O vacancies. The least stable would be Au at a Ce vacancy: ΔG_a is much more positive than those in any other cases considered. We also consider the situations where O and Ce vacancies are present simultaneously. For a CeO_2 vacancy, Au prefers a bridge site

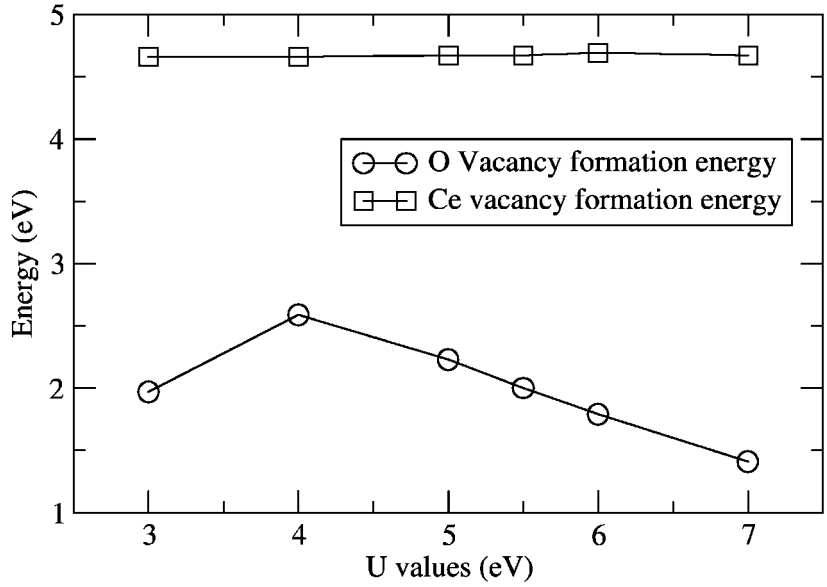

Figure 5. The dependence of O and Ce vacancy formation energies on the U value.

TABLE 1: Vacancy Formation Energies (ΔE_v) and Au Adsorption Energies (ΔE_a) from DFT+U Calculations[a]

	GGA+U						LDA+U:
	U = 3.0	U = 4.0	U = 5.0	U = 5.5	U = 6.0	U = 7.0	U = 6.0
ΔE_v^O	1.97	2.59	2.23	2.00	1.79	1.41	2.28
ΔE_v^{Ce}	4.66	4.66	4.67	4.67	4.69	4.67	4.31
ΔE_a^{stoi}		2.06	1.87	1.75	1.92		1.91
ΔE_a^O		3.16	2.98	2.88	2.78		2.50
ΔE_a^{Ce}		1.73	1.73	1.73	1.73		1.26

[a] The units are eV.

of two subsurface O atoms to either an O vacancy or a Ce vacancy (Figure 4e); for a defect consisting of both an O vacancy and a Ce vacancy, Au binds with four neighboring O atoms (Figure 4d). Adsorption in both cases are stronger than that at a single Ce vacancy.

Figure 3 also shows that only under the most extreme O-rich conditions (e.g. $\mu_O > -0.4$ eV) does Au adsorption at the O vacancy become less favorable than adsorption at the Ce vacancy. However, $\mu_O = -0.4$ eV would require conditions that are highly unlikely to be achieved in the WGS process. For example, to achieve $\mu_O = -0.4$ eV at 400 K, the ratio of the partial pressures between water and hydrogen would be $1:10^{-20}$, which means that no hydrogen is produced; even at a temperature of ~1200 K, the partial pressure ratio needs to be $1:10^{-10}$ for water and hydrogen. In addition, under the O-rich conditions, the adsorption at a defect consisting of an O vacancy and a Ce vacancy, and even the adsorption at the stoichiometric surface, would be more favorable than the adsorption at a Ce vacancy site. Returning to the argument of the anchoring site being on an O vacancy or a Ce vacancy, our thermodynamic data is therefore firmly in favor of the oxygen vacancy model. Furthermore, our results suggest that not only a single O vacancy but also O vacancy clusters could be the anchoring sites for a Au cluster, because of the similar ΔG_a values obtained. This finding is potentially significant, because the vacancy clusters would direct the Au cluster into specific shapes that may have advantages in catalysis, and groups of Ce^{3+} ions in the vicinity of vacancy clusters would also be exposed to the adsorbates and consequently could play some interesting catalytic roles.[42] Understanding the formation mechanism and nature of O vacancy clusters, which we are currently pursuing, would therefore be useful.[43]

C. Effects from Methodologies. Finally, we illustrate the effects from different U values (U = 3.0, 4.0, 5.0, 5.5, 6.0, and 7.0 eV) and different DFT functionals (GGA+U and LDA+U). We compute vacancy formation energies (ΔE_v) and Au adsorption energies (ΔE_a), which are each defined in a similar manner to those in eqs 3 and 6, except that μ_O is replaced by half of the total energy of an O_2 molecule. The results are compiled in Table 1.

Considering first the O vacancy formation energy (ΔE_v^O), our results are in good agreement with those reported in the literature. ΔE_v^O from GGA+U (i.e., 2.23 eV when U = 5.0 eV is used) is close to the previously reported energy (2.60 eV),[30] for which the same U value was chosen: the somewhat larger values in the literature are due to the smaller unit cell (i.e., 2 × 2 cell) used. Furthermore, the significant variation of ΔE_v^O with changing U values, as can be seen in Table 1 and Figure 5, was also reported for bulk ceria.[34] A similar trend was produced:[34] the ΔE_v^O values are higher for intermediate U and become lower for smaller and larger U, although the physical origin for these trends is unclear. We should mention that it is beyond the scope of this study to unravel the origin of these variations. Instead, the main point from Table 1 is that despite the significant dependence of ΔE_v^O on U values, compared to ΔE_v^O calculated with U = 5.0 eV, the only increase (i.e., 0.36 eV when U = 4.0 is used) is very small compared to the huge energy difference between creating an O vacancy and a Ce vacancy (over 10 eV in Figure 1), whereas ΔE_v^Ocalculated with other U values all decrease (i.e., O vacancy formation would be more favored). Thus, our conclusions concerning the relative stabilities of the O vacancy and the Ce vacancy would not be affected, provided that the dependence of the Ce vacancy formation energy (ΔE_v^O) on U is not significant. Indeed, Table

1 shows that ΔE_v^O is rather insensitive to the choice of U values. This result is reasonable, because the removal of a Ce atom only leads to electron depletions on the seven O atoms surrounding the Ce vacancy, where f electrons would not be involved.[36] In addition to GGA+U, Table 1 also shows the tests from LDA+U, in which we use $U = 6.0$ eV (the optimal U from previous studies[34,35]). As can be seen, results from LDA+U are quite similar to those from GGA+U ($U = 5.0$ eV).

For Au adsorption, we summarize in Table 1 the adsorption energies on the stoichiometric surface (ΔE_a^{stoi}) and on defective surfaces with either an O (ΔE_a^O) or a Ce vacancy (ΔE_a^{Ce}). We note that the magnitude of variations of ΔE_a^O is smaller than that of ΔE_v^O. This may be attributed to the less-filled f electronic states in the adsorption systems (owing to the electron transfer to the adsorbed Au) than those for the pure surfaces. Like ΔE_v^{Ce}, ΔE_a^{Ce} is also almost independent of U values. Thus, given the large differences (~7.0 eV) between ΔG_a^O and ΔG_a^{Ce} under reaction conditions, these variations would not affect our earlier conclusions.

IV. Conclusions

By applying the ab initio thermodynamics approach, we have computed vacancy formation energies and Au adsorption energies on surfaces with various vacancies. We have established that under WGS reaction conditions, O vacancies are much easier to form and are much more stable than Ce vacancies, and that the addition of Au does not alter the relative stabilities of the two vacancies (although the difference becomes smaller). Because Au strongly prefers the O vacancy site to the Ce vacancy site, we suggest that a Au atom occupying an O vacancy can act as the nucleation site for the growth of nanoparticles. We have also shown that, in addition to a single oxygen vacancy, oxygen vacancy clusters could be the anchoring sites for gold nanoparticles, as Au possesses similar stabilities in these cases.

Acknowledgment. We acknowledge the Cambridge Isaac Newton Trust (C.Z.) and The Royal Society (S.J.J). A.M. is supported by the EURYI scheme (see www.esf.org/euryi) and the E.P.S.R.C.

References and Notes

(1) Haruta, M.; Yamada, N.; Kobayachi, T.; Iijima, S. *J. Catal.* **1989**, *115*, 301.
(2) Bond, G. C.; Thompson, D. T. *Catal. Rev.-Sci. Eng.* **1999**, *41*, 319.
(3) Trimm, D. L.; Onsan, Z. I. *Catal. Rev.-Sci. Eng.* **2001**, *43*, 31.
(4) Andreeva, D. *Gold Bull.* **2002**, *35*, 82.
(5) Fu, Q.; Saltsburg, H.; Flytzani-Stephanopoulos, M. *Science* **2003**, *301*, 935.
(6) Pattrick, G.; Van Der Linger, E.; Corti, C. W.; Thompson, D. T *Top. Catal.* **2004**, *30−31*, 273.
(7) Burch, R. *Phys. Chem. Chem. Phys.* **2006**, *8*, 5483.
(8) Tabakova, T.; Boccuzzi, F.; Chiorino, A.; Manzoli, M.; Andreeva, D. *Appl. Catal., A* **2003**, *252*, 385.
(9) Rodriguez, J. A.; Pérez, M.; Evans, J.; Liu, G.; Hrbek, J. *J. Chem. Phys.* **2005**, *122*, 241101.
(10) Wang, X.; Rodriguez, Hanson, J. C.; Ṕ; erez, M.; Evans, J. *J. Chem. Phys.* **2005**, *123*, 221101.
(11) Sanches, M.; Gazgues, I. *J. Catal. A* **1987**, *104*, 120.
(12) Liu, Z. P.; Jenkins, S. J.; King, D. A. *Phys. Rev. Lett.* **2005**, *94*, 196102.
(13) Tibiletti, D.; Amieiro-Fonseca, Burch, R.; Chen, Y.; Fisher, J. M.; Goguet, A.; Hardcare, C.; Hu, P.; Thompsett, D. *J. Phys. Chem. B* **2005**, *109*, 22553.
(14) Venezia, A. M.; Giuseppe, P.; Longo, A.; Di Carlo, G.; Casaletto, M. P.; Liotta, F. L.; Deganello, G. *J. Phys. Chem. B* **2005**, *109*, 2821.
(15) Chrétien, S.; Metiu, H. *Catal. Lett.* **2006**, *107*, 143.
(16) Shapovalov, V.; Metiu, H. *J. Catal.* **2007**, *245*, 205.
(17) Nolan, M.; Verdugo, V. S.; Metiu, H. *Surf. Sci.* **2008**, *602*, 2734.
(18) Reuter, K.; Scheffler, M. *Phys. Rev. B* **2002**, *65*, 035406.
(19) Michaelides, A.; Bocquet, M.-L.; Sautet, P.; Alavi, A.; King, D. A. *Chem. Phys. Lett.* **2003**, *367*, 344.
(20) Michaelides, A.; Reuter, K.; Scheffler, M. *J. Vac. Sci. Technol. A* **2005**, *23*, 1487.
(21) Zhang, C.; Alavi, A. *J. Am. Chem. Soc.* **2005**, *127*, 9808.
(22) Kresse, G.; Hafner, J. *Phys. Rev. B* **1994**, *49*, 14251.
(23) Kresse, G.; Furthmüller, J. *Comput. Mater. Sci.* **1996**, *6*, 15.
(24) Kresse, G.; Furthmüller, J. *Phys. Rev. B* **1996**, *54*, 11169.
(25) Blöchl, P. E. *Phys. Rev. B* **1994**, *50*, 17953.
(26) Kresse, G.; Joubert, D. *Phys. Rev. B* **1999**, *59*, 1758.
(27) Perdew, J. P. In *Electron Structure of Solids '91*; Ziesche, P., Eschrig, H., Eds.; Akademie Verlag: Berlin, 1991.
(28) Anisimov, V. I.; Zaanen, J.; Andersen, O. K. *Phys. Rev. B* **1991**, *44*, 943.
(29) Rohrbach, A.; Hafner, J.; Kresse, G. *J. Phys.: Condens. Matter* **2003**, *15*, 979.
(30) Nolan, M.; Grigoleit, S.; Sayle, D. C.; Parker, S. C.; Watson, G. W. *Surf. Sci.* **2005**, *576*, 217.
(31) Fabris, S.; Vicario, G.; Balducci, G.; de Gironcoli, S.; Baroni, S. *J. Phys. Chem. B* **2005**, *109*, 22860.
(32) Kresse, G.; Blaha, P.; Da Silva, J. L. F.; Ganduglia-Pirovano, M. V. *Phys. Rev. B* **2005**, *72*, 237101.
(33) Loschen, C; Carrasco, J.; Neyman, K. M.; Illas, F. *Phys. Rev. B* **2007**, *75*, 035115.
(34) Andersson, D. A.; Simak, S. I.; Jahansson, B.; Abrikosov, I. A.; Skorodumova, N. V. *Phys. Rev. B* **2007**, *75*, 035109.
(35) Castleton, C. W. M.; Kullgren, J.; Hermansson, K. *J. Chem. Phys.* **2007**, *127*, 244704.
(36) Zhang, C.; Michaelides, A.; King, D. A.; Jenkins, S. J. *J. Chem. Phys.* **2008**, *129*, 194708.
(37) Stull, D. R.; Probhet, H. *JANAF Thermochemical Tables*, 2nd ed; U.S. National Bureau of Standards: Washington, DC, 1971.
(38) Fabris, S.; de Gironcoli, S.; Baroni, S.; Vicario, G.; Balducci, G. *Phys. Rev. B* **2005**, *71*, 041102.
(39) Kim, C. H.; Thompson, L. T. *J. Catal.* **2006**, *244*, 248.
(40) Andreeva, D.; Idakiev, V.; Tabakova, T.; Ilieva, L.; Falaras, P.; Bourlinos, A.; Travlos, A. *Catal. Today* **2002**, *72*, 51.
(41) Esch, F.; Fabris, S.; Zhou, L.; Montini, T.; Africh, C.; Fornasiero, P.; Comelli, G.; Rosei, R. *Science* **2005**, *309*, 752.
(42) Campbell, C. T.; Peden, C. H. *Science* **2005**, *309*, 713.
(43) Zhang, C.; Michaelides, A.; King, D. A.; Jenkins, S. J. *Phys. Rev. B* **2009**, *79*, 075433.

JP810093A